HELICOPTER FUSELAGE MODEL DRAG REDUCTION BY ACTIVE FLOW CONTROL SYSTEMS

Fabrizio De Gregorio, f.degregorio@cira.it, CIRA (Italy)

Abstract.

A comprehensive experimental investigation of helicopter blunt fuselage drag reduction using active flow control (AFC) is being carried out within the European CleanSky program. The objective is to demonstrate the capability of several active technologies to decrease fuselage drag by alleviating the flow separation occurring in the backdoor area of some helicopters. The work is performed on a simplified blunt fuselage at model-scale. Two different flow control actuators are considered for evaluation: steady blowing and unsteady blowing (or pulsed jets). Laboratory tests of each individual actuator are first performed to assess their performance and properties. The fuselage model is then equipped with these actuators distributed along the loading ramp edges. This paper addresses the promising results obtained during the wind-tunnel campaign, since significant drag reductions are achieved for a wide range of fuselage angles of attack without detriment of the other aerodynamic characteristics.

1. Introduction

The performances of heavy transport helicopters, having a large, and almost flat, loading ramp suffer from the poor aerodynamics of the aft body.

In cruise flight condition, the component of the rotor power due to counter balance the helicopters parasite force is of the order of 45% to 55% of the total requirements depending by the helicopter class, as observed in 1975 by Stroub and Rabbot [1] and later by Gatard et al in 1997 [2]. More recent fuselage and rotor head drag breakdown studies [3], [4], indicate that about the 69% of the total parasite drag can be ascribe to the fuselage and the remaining 31% is due to the rotor head for heavy class helicopters. Further detailed drag breakdown (Figure 1) indicates that the basic fuselage contributes with about 19%, engine cowls by 11%, sponson about 5%, empennage with 7%, tail rotor head, cooling system and Aerials respectively for about 5%, 6% and 16%.
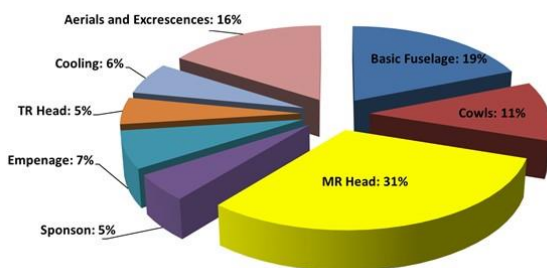

Figure 1. Heavy Class Helicopter parasite drag breakdown

Consequently, fuselage drag reduction is one of the main objectives in order to improve the helicopter performances, to reduce the fuel consumption and the environmental impact. Heavy helicopter fuselages are often characterized by a rear loading ramp that significantly affects the aerodynamic performance. The transport helicopter fuselage can be assimilated to a blunt body and the aft region is typically characterized by a flow detachment at the lower corner, generating a separation bubble and a system of streamwise vortices at the sides. These vortical structures present some similarity to those separated from hatch-back cars [5]. The flow separation and the longitudinal vortex always cohabit on the aft region, when the flow separation is predominant the flow is named "eddy flow" otherwise it is called "vortex flow." The fuselage drag magnitude is strictly influenced by the hatch flow topology, being related with the fuselage incidence angle (α) and with the loading door upsweep angle (ϕ) as widely discussed by Seddon in 1990 [6]. Furthermore, a point not to be neglected is that the flow separation interacting with the fuselage tail induces the airframe to fatigue cycles.

Fuselage drag reduction can be obtained by means of an optimization of the aerodynamic design [7], [8] and [9] by improving the streamlined geometry (for example fishtailed geometry characterized by small upsweep angles ϕ=15° instead of blunt body fuselage with large upsweep angles ranging between 30° to 35°). In alternative, fuselage drag reduction can be pursued by using flow control systems [10] [11], when the operative requirements prevent substantial modifications of the fuselage geometry or the retrofit of existing rotorcraft is required.

During the last years several research teams investigated the possibility to reduce helicopter fuselage parasite drag by means of active flow control (AFC) systems. In 2005, Martin et al. [12] investigated numerically and experimentally the influence of 12 synthetic jet (SJ) actuators on a helicopter fuselage obtaining drag reduction in the range between 6 and 10% and estimating the possibility to reduce of almost the 40% the lift download. Analogous results were obtained by Ben-Hamau et al in 2007 obtaining drag reductions in the range between 3 to 11% for different attitudes and yaw angles [13] using blowing coefficient values ($C\mu$) ranging between 0.025 to 0.05. In 2010, a NASA and ONERA [14] collaboration investigated numerically and experimentally the behavior of different AFC systems (steady blowing and SJ), obtaining remarkable result in drag reduction, with the steady blowing system able to reduce up to 35% the fuselage drag at $C\mu$: 0.06 and the synthetic jets inducing a decrement up to 26% operated at $C\mu$: 0.038. A contribution to understand the AFC influence on the helicopter fuselage has been provided by Le Pape et al in 2013 [16] with their comprehensive work investigating the effect on the fuselage drag and lift download. A further promising control system is the COMPACT (Combustion Powered actuation) [17], a novel

technology which exploits the chemical energy of gaseous fuel/oxidizer mixture to create a high pressure burst and subsequent high momentum jet of exhaust products. In 2011 the chemical powered actuators were investigated by George et al [18] and by Woo et al [19] on a ROBIN fuselage model obtaining a drag reduction of the order of 12 to 17 % but also a significant increment of the lift download. The authors claimed that the COMPACT actuator is the possible solution to overcome the shortage of momentum of the SJ based on piezoelectric membranes. Another interesting actuator is the fluid oscillator investigated by Martin et al [20] on the ROBIN fuselage equipped of powered rotor. The results indicated, in some cases, a reduction of the total drag of the order of the 20% respect the baseline configuration.

Although many effort have been made in the past, there is still a large interest and different flow control systems are being investigated in order to increase the fuselage performance. Additional efforts are necessary in order to understand the interaction between the flow topologies and the selected actuators. Previous experiments duly investigated the fuselage behavior for different attitude angles but many presented some shortcomings regarding the influence of the yaw angle on the effectiveness of the flow actuators and few discussed the effect on the lift download and on the pitching moment.

This research was driven by the interest to understand the flow topology of an heavy transport helicopter fuselage and in what manner it could be possible to obtain a drag reduction by using steady and unsteady blowing (or pulsed jet) actuators without penalizing the other aerodynamic characteristics.

As initial activities, a comprehensive experimental and CFD investigation was conducted at laboratory level on a small simplified fuselage model equipped by steady blowing and pulsed jets at a Reynolds number based on the fuselage length of about 1 million [21]. The investigation provided a clear picture of the flow characteristics in the region of the loading ramp for different values of the incidence angle. The Wind Tunnel Test (WTT) delivered a better understanding of the effect of the steady and pulsed jets in alleviating the pressure drag inducing flow reattachment and deflecting the longitudinal vortex path. Furthermore, fundamental indications regarding the position and the direction of the jet slot were gathered.

This research foresees the experimental assessment of the flow control systems on a heavy class helicopter fuselage model at larger Reynolds number (Re: $8.2*10^6$). The paper first describes the simplified helicopter model and the wind-tunnel test set-up. A second part is dedicated to the presentation of the different actuators and their property and performance evaluation during specific laboratory tests. Wind-tunnel tests measurements that include aerodynamic loads acting on the fuselage, static pressure taps and PIV measurements are presented and discussed. An overall analysis of the results including actuators comparison with respect to achieved drag reduction is then presented.

2. Experimental Set up

An overview of the investigated test article, wind tunnel, experimental set up, model measurement instrumentation, flow control system and flow velocity measurement system is provided in the following.

2.1. Wind tunnel description

The test campaign was conducted at the RUAG LWTE wind tunnel, an atmospheric closed loop wind tunnel with closed test section.

Test section main sizes are: height of 5 m, width of 7 m and length equal to 11 m. The test section sizes assured negligible wall interferences on the load measurements (Figure 2). The ratio between model cross section and the tunnel test section was 0.45% much smaller of the values of 5% where the wall interference becomes significant and wall corrections are necessary [22].

Figure 2: Fuselage model in WT test section

Maximum achievable wind tunnel speed is 70 m/s with a turbulence level of 0.3% on longitudinal velocity and 0.15% on the lateral velocity at 65 m/s. The full test campaign was carried out at constant speed of V_∞=50 m/s and Reynolds number, based on the fuselage length, of $8.2*10^6$. The fuselage was investigated varying the incidence angle in sweep mode between -12° to +16° at fixed yaw angle of β=0° and β=-5° and sweeping the yaw angle β between -15° to +15° at fixed incidence angle of α=0 and at cruise flight incidence angle of α=-3°. The model was mounted in the up-right position and supported by the dorsal strut in order to minimize disturbances in the regions of interest.

2.2. Simplified fuselage Model

The investigation was carried out on the basic fuselage model of a well-known heavy class helicopter. The terms basic fuselage indicates that sponsons, cowls, empennage, landing gears, rotor head and aerial excrescences have been removed. The tested model is geometrically scaled 1 to 7 respects the full scale vehicle and is characterised by a rear loading ramp having an up-sweep angle of ϕ=32°. The model is composed by an internal structure on which are mounted the external fuselage surfaces and the measurement instrumentations.

The model is equipped by 135 pressure taps. The pressure taps location is shown in Figure 3. The pressure taps are located on the model nose, on the plane of symmetry, on several waterlines (y/H= 0, 0.26 and 0.54 where H is the fuselage height) and on the aft region at different stations (x/L=0.64, 0.68, 0.72, 0.75, 0.81 and 0.86 where L is the fuselage length) along the loading ramp and the tail boom. A single transition strip is placed on the nose cone to facilitate the laminar to turbulent transition on the fuselage.
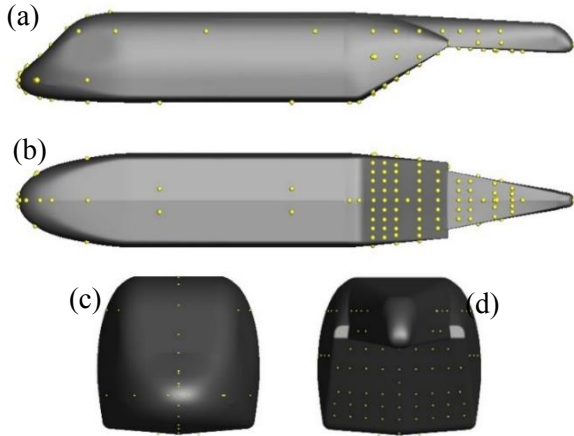
Figure 3: Model PTS location: lateral view (a), bottom view (b), front view(c) and rear view (d).

2.3. Model Instrumentation

The aerodynamic loads were measured by an internal six components balance, Main characteristics in terms of full scale and accuracy are summarised in *Table 1*. The balance was installed in the model central part on a steel plate as close as possible to the mass centre.

Table 1: Balance type 192 RUAG main characteristics

	Fx [N]	Fy [N]	Fz [N]	Mx [Nm]	My [Nm]	Mz [Nm]
Full scale	350	250	1200	100	120	130
Accuracy	0.4	0.7	0.9	0.02	0.02	0.06

Two inclinometers with accuracy of 0.03° degree were installed to measure the pitch and roll attitude of the wind tunnel model. The yaw angle position was provided by the rotating model support. In addition, an electrolevel was used to reliably and quickly set the model to the zero reference pitch attitude and a further MEMS inclinometer was placed as backup. All these instrumentations were mounted on the aluminium plate available on the front of the fuselage (**Figure 4**).
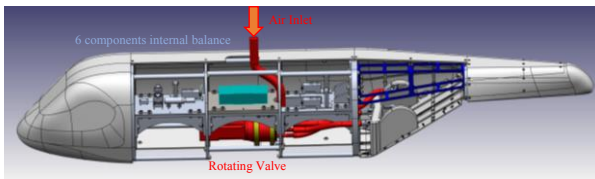

Figure 4*:* Model with instrumentation and flow control actuators iso-view

A total of three ESP modules with 64 ports each full scale value of 6895 Pa (1 psi) and an accuracy of 0.03 % FS were used for measuring the 135 pressure ports. One pressure transducer was mounted on the front part of the model to cover the nose pressure taps while the remaining two were mounted in proximity of the model aft where the PTS are concentrated.

2.4. Flow control system description

The simplified fuselage model was designed in order to present five actuator slots in the loading ramp region,

three crosswise directed and located on the bottom of the ramp. Each bottom slot is characterised by length and width respectively of L_{jB}:105 mm and W_{jB}: 1.8 mm and directed respect with the ramp surface of a jet angle of α_{jB}=-37°.

The lateral slots are directed outboard of α_{jL}=45° respect with the surface plane in order to delay the vortex flow roll up, the slot length and width are respectively of L_{jL}:170 mm and W_{jL}:1.8mm. The AFC system foresees two geometry configurations (Configuration 1 and Configuration 2).

In the first configuration (AFC1), the rotating valve feeds the three bottom slots (left image of *Figure 5*). The second configurations (AFC2) contemplates that the blowing circuits are connected to the lateral slots together with the central bottom slot as shown in the right image of *Figure 5*.

Figure 5: AFC first configuration (left image), second configuration (right image).

Two different AFC systems are considered: steady blowing and pulsed jet operating from the rear bottom slots.

The steady blowing jet is obtained feeding the cavity by external air supply through the model allowing several flow rates and blowing velocities to be tested.

The pulsed jet is achieved modulating the supplied mass flow by means of a rotating valve. The rotating pneumatic valve consists of two concentric cylinders. The inner cylinder (or rotor) rotates around its axis of revolution driven by an electrical stepper motor. The outer cylinder (or stator) is fixed. The inner cylinder contained 7 apertures with diamond shape and equally angular spaced ($\Delta\varphi$=51.43°) on the same circumference. The outer cylinder contains 3 circular apertures along the circumference and in correspondence of the rotor apertures. The air transfer is obtained when the rotor apertures aligns with the stator apertures.

The pulse frequency f_j is calculated multiplying the rotating speed by the number of rotor apertures $f_j=\omega*Ns$. Varying the rotating speed and the flow rate is possible to change the jet frequency and the blowing jet speed (V_j). Figure 4 shows the rotating valve, inlet and outlet, tube routing and the plenum chambers mounted inside the model. The rotating valve supply the pressurised air to the three slots at the same time. A strong Coanda effect induces the jet flow attachment to the rear ramp (*Figure 5*).

2.5. Flow Measurements

The flow field characteristics downstream of the fuselage aft region were investigated by two PIV measurement systems: a standard two components PIV system and by a stereo PIV system. The S-PIV measurements were carried out at three different vertical cross planes at

different distances from the model nose (x/L=0.75, 0.81, and 0.86) and respectively named PIV1, PIV2, PIV3. The 2C-PIV measurements were performed on the symmetry plane (y/W=0) downstream the loading ramp and indicated as PIV4. The measurement planes are shown in Figure 6.
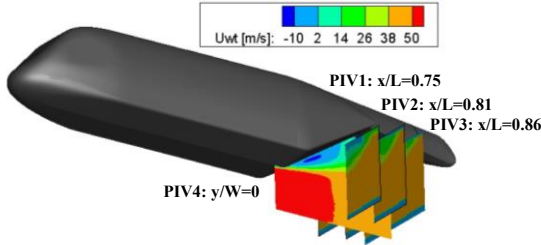

Figure 6: PIV recording region

The S-PIV system was composed of two Nd-Yag resonator heads providing a laser beam of about 320 mJ each at 532 nm and by two double frame CCD cameras (2048x2048 pixels) whereas the 2C-PIV system was composed of two Nd-Yag resonator heads providing a laser energy of about 200 mJ each at 532 nm and by a single PIV sCMOS sensor camera (2560x2160 pixels).

Particles of about 1 μm of diameter, composed of DEHS oil, were used as seeding. The seeding was injected downstream of the test section in order to obtain uniform seeding concentration of the full circuit. The lasers were located under the test section. The laser light sheet was projected upward into the test section trough an acrylic window installed in the test section floor.

Each recording camera belonging to the S-PIV was located outside of the test section, inside the door frames of the side wall rear doors, downstream of the model. The working distance for each camera was nearly 6.7 meters. This distance, coupled with the camera angle and sensor size resulted in a field of view of approximately 510 mm by 395 mm (width x height). Based on the camera sensor size, the magnification was estimated to be 0.233 mm/pixel and a spatial resolution of 5.58 mm^{-1}.
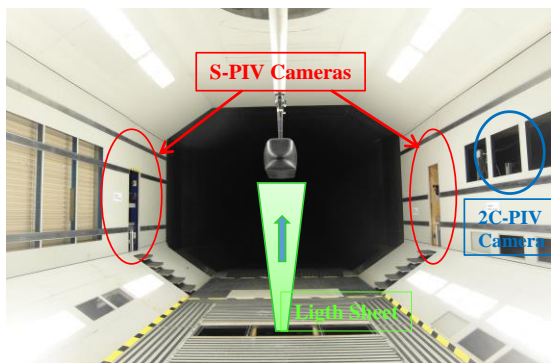

Figure 7: PIV recording lay-out in WT test section.

The 2C-PIV camera was mounted outside the left lateral wall behind a windows at a distance of about 2.8 meters. The 2C-PIV field of view was approximately 694 by 585 mm^2 with a magnification of 0.271 mm/px and a spatial resolution of 6.5 mm^{-1}. The PIV systems lay-out is illustrated in *Figure 7*.

3. Active Flow Control laboratory characterization.

Before the wind tunnel test campaign, particular care was taken for characterising the steady blowing and pulsed jet pneumatic system. A dedicated laboratory test campaign was aimed to obtain the transfer function relating the flow volume rate to the mean and maximum jet velocity for each single slot.

The flow rate was measured by a flowmeter model SD8000 with measuring range between 0.25 to 225 m^3/h and accuracy equal to the 3% of the FS. The flow velocity at the different slot exit was measured by means of an IFA300 constant temperature anemometer system using single and double wire sensors.

The steady blowing jet speed was measured varying the volume flow rate. Analogous the velocity time history was measured varying the jet frequency and the volume flow rate for the pulsed jet actuators. The results indicate an almost linear behaviour of the mean jet speed varying the flow rate for the case of the steady blowing actuators (*Figure 8*). The pulsed jet characterization presents similar behaviour for the mean velocity while an influence of the jet frequency is evident on the maximum and minimum velocity. The diagram shown in *Figure 8* presents a reduction of the velocity amplitude increasing the jet frequency. The pulsed jet induces an increment of the maximum speed of about the 30-35% respect the steady jet for the same flow rate.
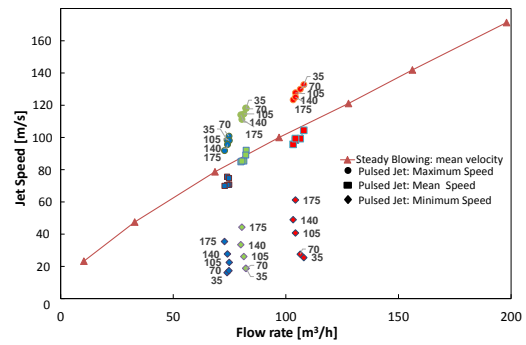

Figure 8: Jet speed (Vj) vs flow rate. Steady blowing speed is indicated by triangle markers, the pulsed jet maximum, mean and minimum speed are indicated respectively by circle, square and diamond markers. Nearby the pulsed jet marker the jet frequency is indicated.

Once that the steady and pulsed jet were characterized in term of mean and peak velocity in the full achievable frequency range it was possible to calculate the characteristic non dimensional quantities defined for evaluating the flow control systems [10]. In particular the jet frequency normalised as:

$$F^+ = f_j \cdot W / V_\infty$$

where f_j is the pulse jet frequency, W the fuselage width and V_∞ the free stream velocity and the blowing momentum coefficient c_μ, defined as the sum of the contribution of each blowing jet:

$$c_\mu = \frac{\sum_j \rho_j A_j V_J^2}{A_{CS} 0.5 \rho_\infty V_\infty^2}$$

where A_j, ρ_j and V_j are respectively the actuator slot surface, flow density and maximum jet speed and A_{cs}, ρ_∞ and V_∞ are the fuselage cross section, free stream density and velocity. The AFC laboratory characterization provided the table with the achievable non dimensional parameters reported in Table 2.

Table 2: AFC normalised parameters

Parameters	range
Reduced Frequency < F$^+$>	0.15 – 1.4
Blowing momentum coefficient <cμ>	0.02 – 0.1
Number of slots	5

4. Test Matrix

The test matrix foresaw first the investigation of the aerodynamic behaviour of the baseline model without AFC system varying the angle of attack at fixed yaw angle and for prefixed values of the angle of attack varying the yaw angle. The model incidence angle was varied in the range between -12° to +16° in sweep mode with an angle resolution of 0.1° at $\beta=0$ and $\beta=-5°$. Similarly the fuselage behaviour was investigated varying the yaw angle in sweep mode from $\beta=-15°$ to $\beta=15°$ at fixed attitude: null angle of attach ($\alpha=0°$) and cruise condition ($\alpha=-3°$).

Once that the baseline behaviour was assessed, the influence of the steady and pulsed jet was investigated varying the flow control parameters for all the selected incidence angles in the operating range reported in Table 3.

Table 3: Investigated AFC values.

Actuators	Flow Rate [m³/h]	Cμ [-]	fj [Hz]	F$^+$ [-]
Steady Blowing	50-60-80	0.005-0.007-0.012	-	-
Pulsed Jet	50-60	0.008-0.012	140	1.14

5. Results

The wind tunnel flow quality and experimental set up provided a very high quality measurements, and an excellent test repeatability. The comparison between the aerodynamic forces and moments coefficient show a fairly good agreement. For example the drag coefficient discrepancy was much smaller of the CD accuracy $\pm 0.4 \cdot 10^{-5}$.

5.1. Baseline

The basic fuselage model was considered as baseline configuration and compared with the different flow control systems. The alpha sweep polar were carefully investigated (Figure 9). For confidentiality reason the discussion of the results is carried out normalizing the aerodynamic coefficient with respect to their values at null incidence angle (CD$_0$, CL$_0$ and CMY$_0$).

The normalized drag coefficient indicates a reduction varying the model incidence from $\alpha=-12°$ to about $\alpha=-5°$. Here the curve slop decreases in concomitance with the occurring of the flow separation on the loading ramp for reaching a minimum value at about $\alpha=+3°$. Further increasing the angle of attack, the drag shows a continuous increment up to $\alpha=+11.4°$ where an abrupt reduction is present with a minimum at about $\alpha=12.10°$. At this point, the flow is fully attached. Increasing the angle of attack the drag coefficient presents a positive slope with a marked Cd growth. The normalized lift coefficient shows a constant positive slope along the full sweep range, characterized by a slope reduction in the region affected by the flow separation. Similarly the flow separation region is visible also in the pitching moment behavior, where the curve slope increases in the range between $\alpha=-5°$ to $\alpha=12°$.
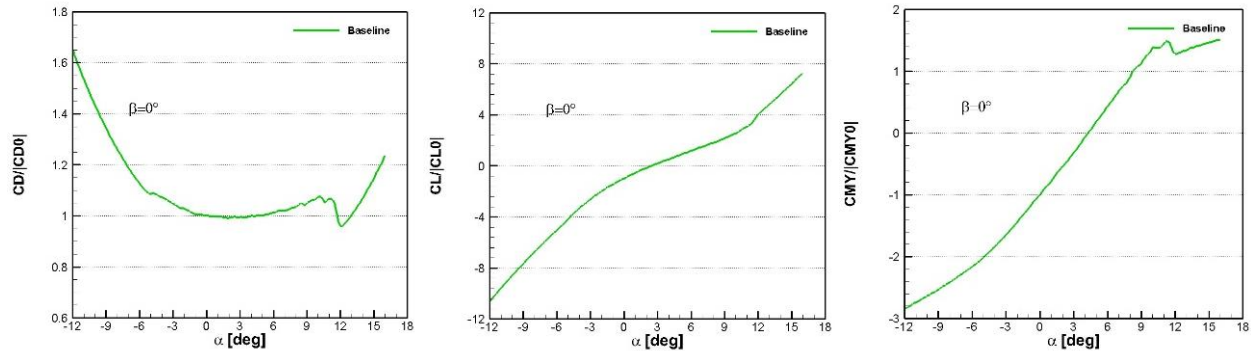

Figure 9: Baseline aerodynamic characterization: normalised drag, lift and pitching moment coefficient with respect to the corresponding values at $\alpha=0°$ varying the incidence angle at $\beta=0°$.

The surface pressure distribution measurements provide valuable information of the flow behavior. The longitudinal pressure distribution indicates the incidence angle range where the eddy flow condition occurs. For the cases of $\alpha \leq -5°$ and $\alpha \geq 12°$, the pressure coefficient presents a marked expansion in concomitance of the sweep angle followed by a pressure recovery along the length of the model, indicating a fully attached flow (solid lines in Figure 10).

For the fuselage attitude interval between -5°<α<12°, the pressure coefficient shows a weak expansion at ramp bottom followed by a constant value confined between x/L=0.63 to x/L=0.68 indicating separated flow on the ramp. Furthermore, the pressure behavior indicates that increasing the incidence angle the separated region presents an increment (dashed lines in *Figure 10*). This Result is confirmed by the flow velocity measurement on the rear ramp symmetry plane. At $\alpha=-3°$, the ensemble average velocity field colour map shows a recirculating region extending from the bottom edge of the fuselage to about the 70% of the loading ramp. As the angle of attack is increased, the flow separation presents a growth up to reach at $\alpha=+7.3°$ the tail boom (*Figure 12*).

The span wise pressure distribution (Figure *11*), together with the cross flow measurement (*Figure 13*), provides a clear indications about the flow topology. At α=-8°, the spanwise pressure distribution at different stations (x/L=0.64, 0.68, 0.72, 0.75 and 0.86) shows a pressure recovery moving along the x direction, indicating an attached flow. Along the spanwise direction an expansion toward the fuselage edge is encountered suggesting the presence of two longitudinal counter rotating vortices. At α=-3° and α=0°, the pressure distribution shows at the first two stations a straight constant values representative of the presence of flow separation. Moving downstream the ramp, the pressure

coefficient indicates a flow reattachment and the presence of longitudinal vortices appears. At α=12° straight span wise distributions indicate the absence of vortex flow and the pressure recovery suggest a fully attached flow.

Also in this case the pressure indications are confirmed by the PIV results (Figure 13). For angle of attach of α=-3°, the cross flow vorticity map indicates the presence of separated flow and two counter rotating vortices. Similar flow behavior is encountered at α=0°and at α=+4.5° but characterized by weaker vortices. Flow velocity map at α=+7.3° indicates the absence of vortex flow.
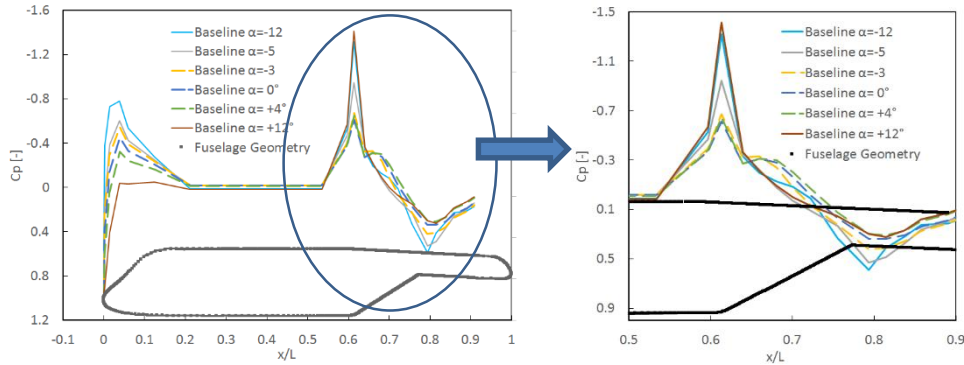
Figure 10: Baseline longitudinal Cp distribution at different incidence angles and fixed β=0°.

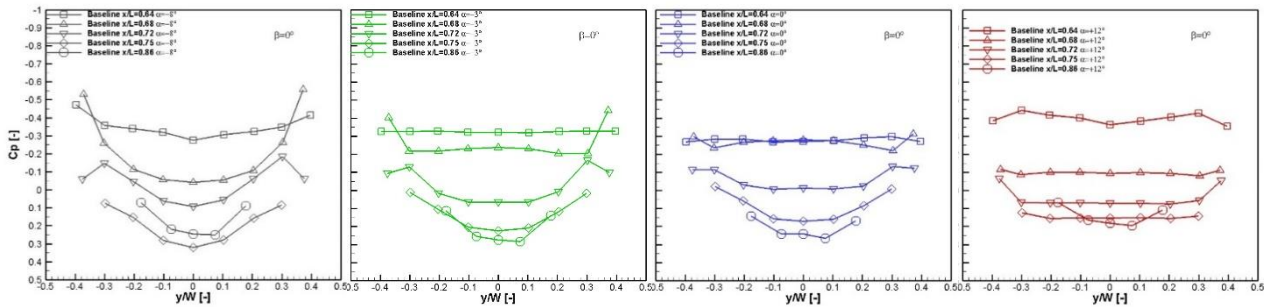Figure 11: Baseline crosswise pressure distribution at different incidence angles. Left diagram α=-8°, central diagram α=0° and right diagram α=12°.

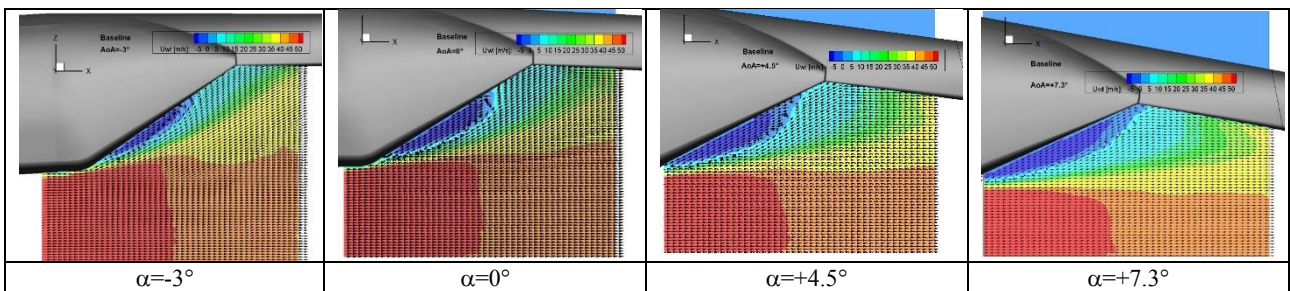| α=-3° | α=0° | α=+4.5° | α=+7.3° |

Figure 12: Baseline flow velocity contour map at different incidence angles. Longitudinal plane PIV4

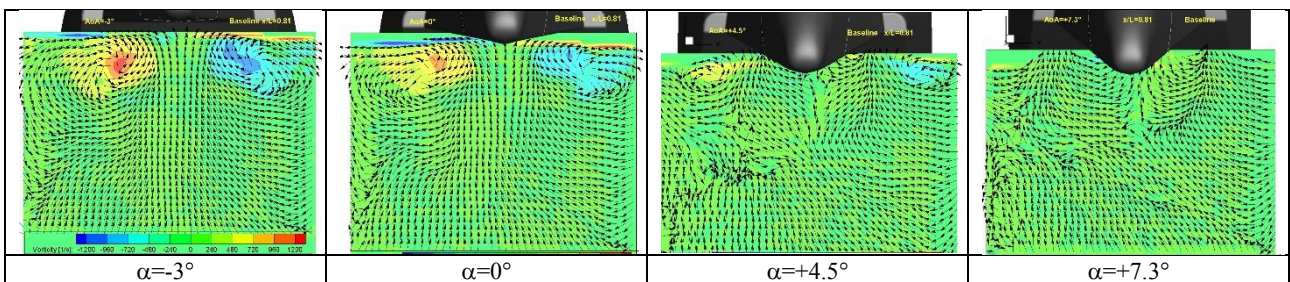| α=-3° | α=0° | α=+4.5° | α=+7.3° |

Figure 13: Baseline flow vorticity contour map at different incidence angles. Crosswise plane PIV2

The helicopter are often operated in side flow conditions. For this reason the fuselage behaviour was investigated sweeping the yaw angle between -15°<β<+15° at constant values of the incidence angle (α=-3° and α=0°). The drag coefficient presents a symmetric behaviour whereas the lift and pitching moments presents an hysteresis contribution. The side flow increases the fuselage drag. A clear loss of symmetry is evident in the wake released by the fuselage for β=-5° respect to the case of β=0° (*Figure 15*). The longitudinal vortices trajectory is deviated pushing the right vortex upward and downward the left one.
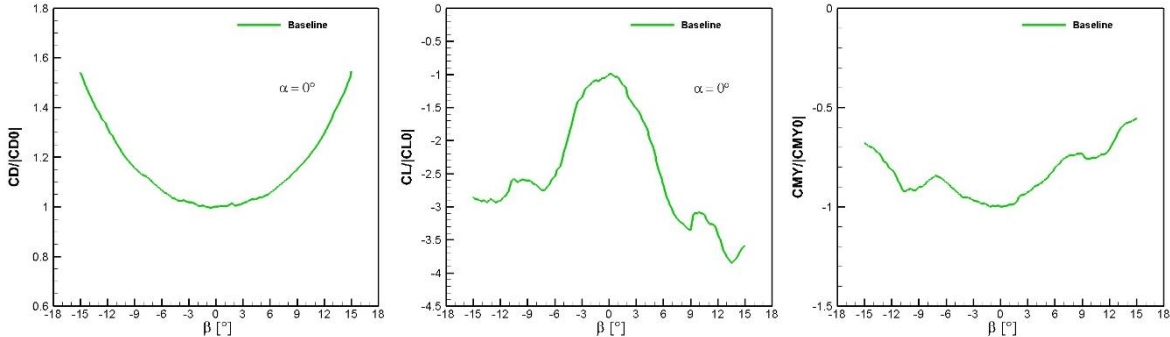
Figure 14: Baseline normalised drag, lift and pitching moment coefficients versus beta sweep angle at α=0°.
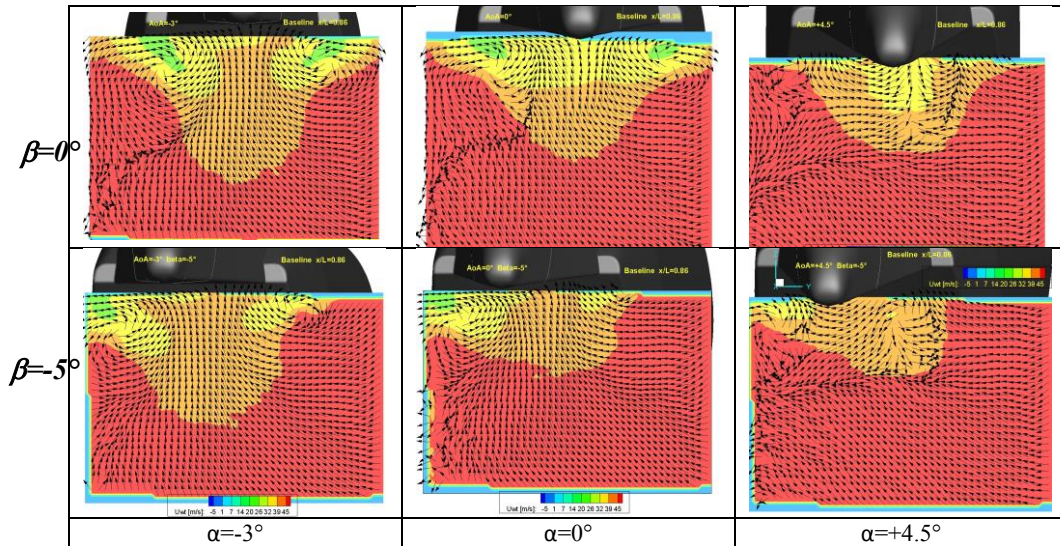
Figure 15: Baseline crossflow velocity contour map at x/L=0.86 for different incidence angle α=-3°, α =0° and α=4.5° respectively at β=0° (upper row) and β=-5° (lower row).

5.2. AFCs Characterization

An additional characterization of the AFC systems was carried out directly in the wind tunnel before starting the test. For the steady blowing system, the volume flow rate was varied taking constant the free stream velocity (V∞=50m/s), incidence angle (α=0° and -3°) and yaw angle null. The pulsed jet was characterised at frequency of f_j=140 Hz and same free stream velocity and model attitude of the steady blowing case.

Both configuration were characterised. The second configuration (AFC2) showed a highly unstable behaviour affected by large drag rise and strong hysteris (black line in Figure 16). This suggested to test mainly the AFC1 although some interesting results obtained by the AFC2 configuration shall be discussed.

Once that the data were corrected by the balance crossing interference, the influence of the AFC1 system on the drag coefficient is obtained (Figure 16). The diagram presents the Cd behaviour versus the volume flow rate for the case of steady blowing actuator and pulsed jet at α=0° and β=0°. Three zones can be selected in the drag coefficient behaviour for the steady blowing jet.
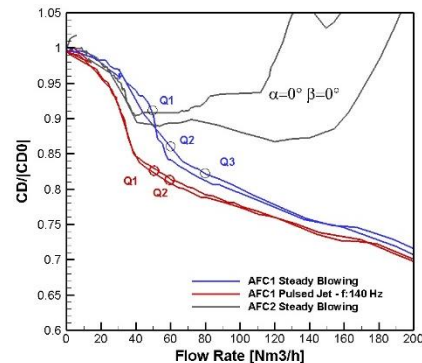

Figure 16: AFC1 characterization: at β=0°, (blue line steady blowing and red line pulsed Jet)

A first zone where the drag start decreasing with a light slope influenced by the effect of the AFC system (flow

rate range between Q=0 m³/h to Q=30 m³/h), a second region characterised by a deeper slope where the flow reattachment is induced (flow rate range between Q=30 m³/h to Q=60-70 m3/h), and a third region characterised by a smaller constant slope where the drag reduction is due to the continuous contribution provided by the blowing slots (flow rate range between Q>60-70 m³/h to Q=200 m³/h). In this last region the additional blowing cost do not provide benefit in the pressure distribution as already investigated in the laboratory scale test campaign [21]. Similar behaviour is encountered for the pulsed jet curve except that the region ranges are different. It is worth to note that the pulsed jet presents a stepper curve suggesting a better efficiency in reducing the drag coefficient. The diagrams were used for selecting the operative values of the active flow control system (*Figure 16*).

5.3. AFC1: Steady Blowing Actuator Results

The experimental assessment of the AFC systems in terms of drag reduction was the main scope of the project. At the same time, it was of great importance to verify that the benefits obtained by the drag alleviation were without detriments to the other quantities in particular lift and pitching moment coefficients.

Three different values of the blowing flow rates were investigated respectively to $C\mu$=0.005, 0.007 and 0.012 (corresponding to Q=50, 60 and 80 m³/h). In the full incidence angle range (from α=-12° to α=+16°), the diagram of the drag coefficient presents a clear benefit in terms of drag reduction varying from 5 to 22 % with respect to the baseline configuration (left diagram in *Figure 17*). The case characterised by a flow rate of Q_1=50 m³/h corresponding to cμ=0.005, shows a drag alleviation although the data still indicate that flow separation occurs in the range between α=-2° to α=+11°. The drag reduction is further enounced for Q_2=60 m³/h ($C\mu$=0.007), but still limited flow separation occurs in the range between α=0° to α=+10°. The larger flow rate value (Q_3=80 m³/h corresponding to $C\mu$=0.012) provides the best behaviour inducing a full flow reattachment on the fuselage as indicated by the pink curve.

The steady blowing system presents a positive effect on the lift coefficient as well. The steady blowing results indicate a benefit in terms of lift download reduction up to 70% for almost all the attitude angles except in the range between α=-5° to α=+1° where a maximum price of about 22% is paid in terms of download increment (central diagram in *Figure 17*).

Some consideration can be drawn also regarding the effect of the steady jet on the pitching moment behaviour. Mostly the pitching moment coefficient decreases with respect to the baseline and it presents an advantage in term of longitudinal stability.

In detail the effect of the steady blowing actuators is described by the longitudinal and spanwise pressure distribution on the lower rear region (*Figure 18*). The longitudinal pressure distribution shows a pressure recovery with respect to the baseline behaviour as the blowing coefficient increases. The lower value of the blowing coefficient is not sufficient to induces the flow reattachment partially obtained with $C\mu$=0.007 and fully reached using $C\mu$=0.012. The flow velocity map on the fuselage symmetry plane at α=-3° confirms this behaviour. The baseline presents a noticeable flow separation on the loading ramp, that almost disappears activating the steady blowing actuators at $C\mu$=0.007 (Figure *23*). Just a limited circulation bubble is located on the conjunction between the ramp and the tail boom.

The spanwise distribution at x/L=0.68 and 0.72 confirms the pressure recovery and the presence of two longitudinal vortices, characterised by two expansion peaks (*Figure 18*). At x/L=0.68, the spanwise pressure distribution shows a pressure recovery and a shape modification from a flat distribution suggesting separated flow to a round distribution indicating attached flow. At x/L=0.72 pressure distribution indicates a reduction of the expansion peaks due to the steady blowing actuators justifying the reduction of the fuselage pressure drag. The crosswise PIV plane at x/L=0.81 shows a fully attached flow and the presence of the two counter rotating vortices shedding by the fuselage. The streamwise velocity component indicates a marked reduction of the released wake (Figure 24). The steady blowing actuators induced an increment of the intensity of the longitudinal vortices and a deflection of the vortex trajectory moving slightly apart by the symmetry plane (Figure *25*).

The actuator effectiveness is demonstrated also on the sweep beta polar carried out at α=0°. The drag coefficient presents a reduction ranging between 6% to 16%. The lift download is characterised by an increment up to a maximum value of 50% in the incidence range between α=-4° to α=+5° and a marked reduction up to 70% on the rest of the angle range. The pitching moment coefficient presents for the complete range of the yaw angle a reduction (Figure 19).
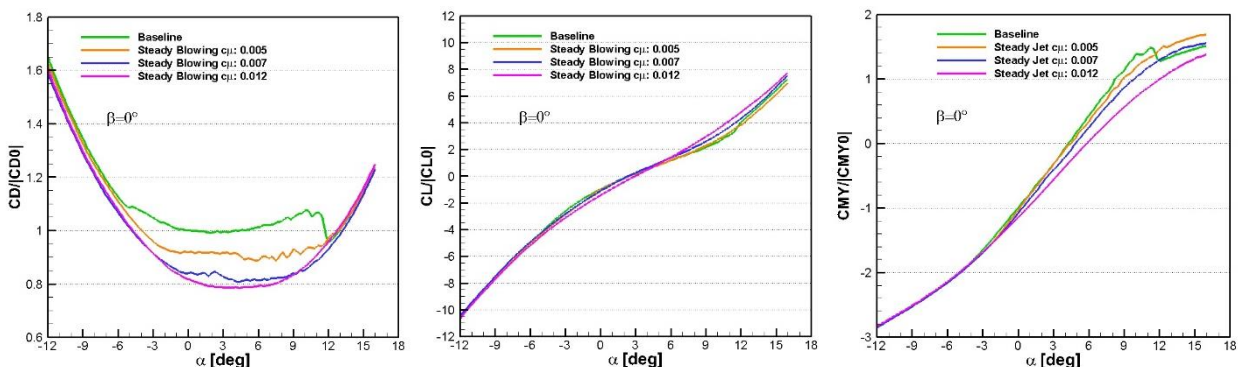

Figure 17: Steady blowing actuator contribution on the normalised aerodynamic coefficients
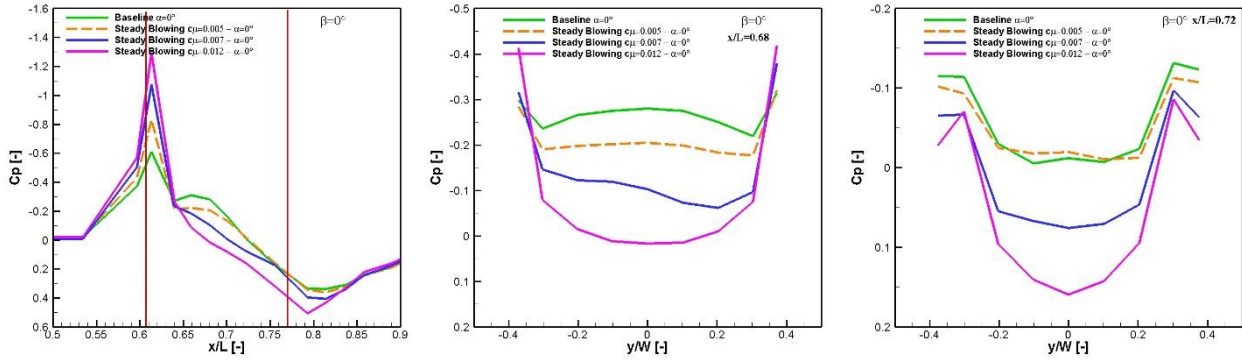
Figure 18: Steady blowing contribution to pressure distribution. Longitudinal and spanwise behaviour.
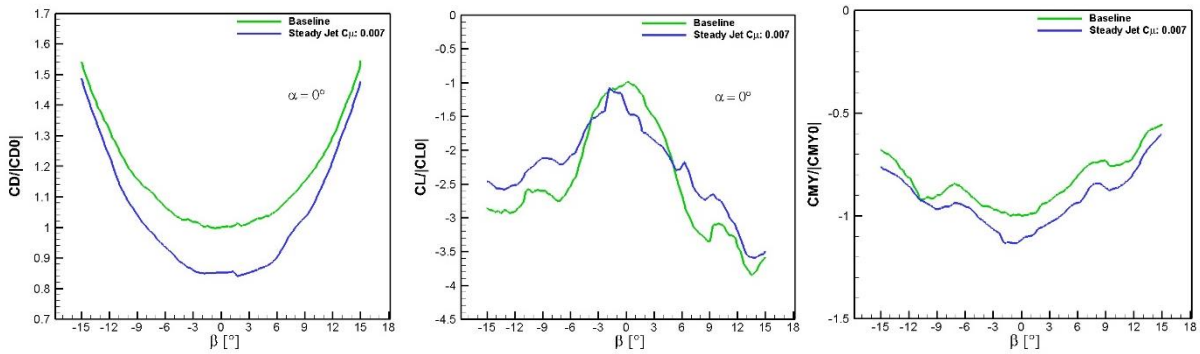

Figure 19: Steady blowing effect on the sweep yaw angle polars.

5.4. AFC1: Pulsed Jet Actuator Results

Main characteristic of the unsteady blowing with respect to the steady blowing actuator is that provide larger blowing coefficient at parity of used flow rate. In the following the discussion is centred on the pulsed jet assessment at flow rate of Q=60m^3/h corresponding to a blowing coefficient of Cμ=0.012, value obtained by the steady blowing actuator operating at flow rate of Q=80m^3/h.

The drag coefficient indicates a reduction with respect to the baseline ranging between 4% to 24% along the full incidence sweep. The pulsed jet although is fed by a flow rate quantity smaller of the 25% has almost the same behaviour if not slightly better with respect to the steady blowing system (Figure *20*). Analogous to the steady blowing behaviour the lift coefficient presents an improvements with respect to the baseline up to 100% for α<-7 and α>+6 and a lost in terms of download increment up to a maximum of 50%. The pitching

moment coefficient shows a reduction of the diagram slopes indicating an increment of the longitudinal stability.

The longitudinal and spanwise pressure distributions show a flow reattachment induced by the activated pulsed jets (Figure 21). The pressure track of the steady and pulsed jet are almost equivalent up to x/L=0.72. Downward the additional flow rate quantity of the steady blowing actuators further forces the pressure recovery. The wake investigation downstream the rear part of the fuselage provides similar results that for the steady blowing actuators. The flow separation is reduced and almost removed by the pulsed jets except on the corner between the loading ramp and the tail boom (Figure *23*). The released wake is reduced, the low streamwise velocity region is limited to a small stripe connecting the counter rotating vortices (Figure 24).
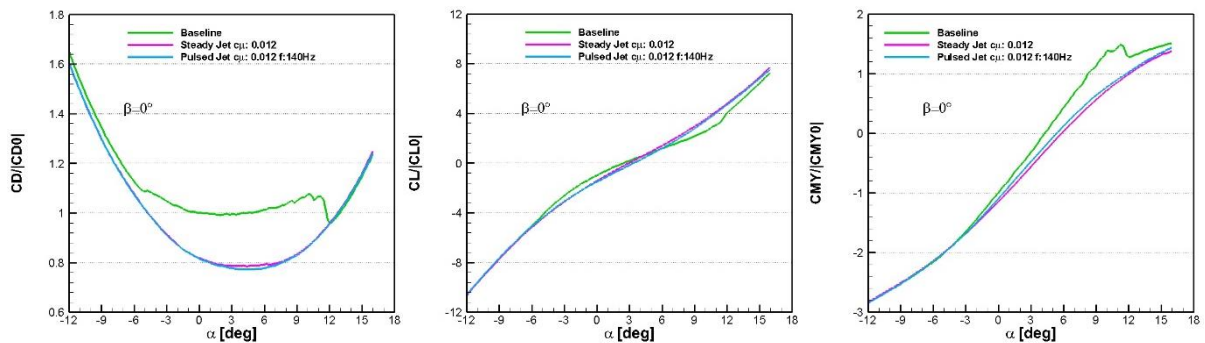

Figure 20: Pulsed jet and steady blowing contribution on the normalised aerodynamic coefficients.
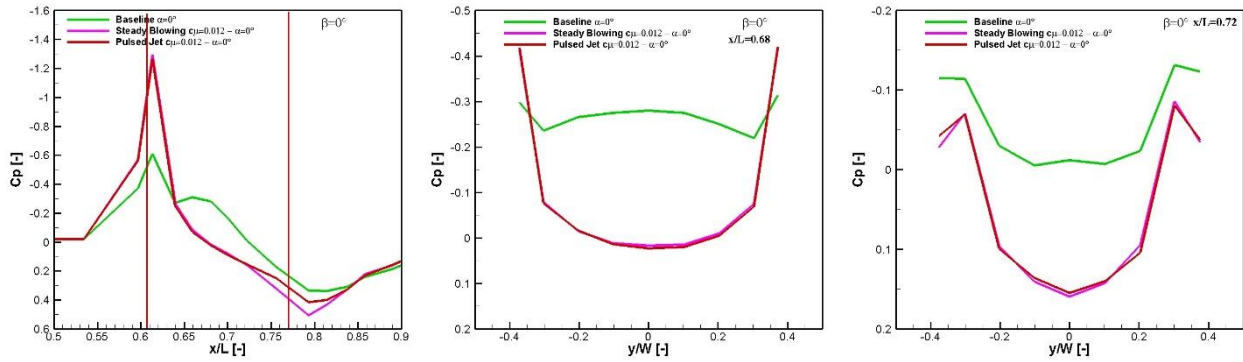
Figure 21: Pulsed Jet and Steady Blowing contribution to longitudinal and spanwise pressure distribution.

The longitudinal vortex flow detected on the cross plane at x/L=0.81 presents a behaviour similar to that one induced by the steady blowing. Larger vorticity intensity and vortex core displacement moving apart from the symmetry plane (*Figure 25*).

The pulsed jet effectiveness is demonstrated also on the sweep beta polar carried out at α=0°. The drag coefficient presents a reduction ranging between 8% to 20% with respect to the baseline configuration and a

better behaviour regarding the steady blowing. The lift download is characterised by an increment up to a maximum value of 70% in the incidence range between α=-5° to α=+5.5° and a marked reduction up to 80% on the rest of the angle range. The pitching moment coefficient presents for the complete range of the yaw angle a reduction (*Figure 22*). The wake measurements indicated a reduction of the momentum loss induced by the flow control system showing a reduction of the wake size (Figure 26)
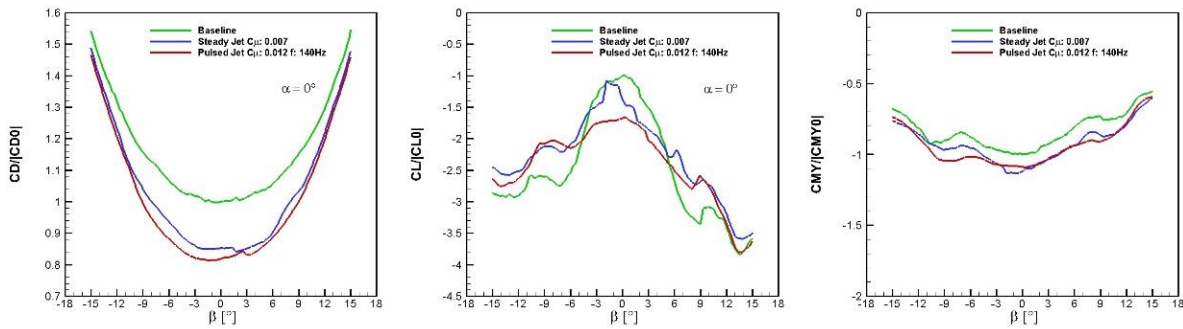

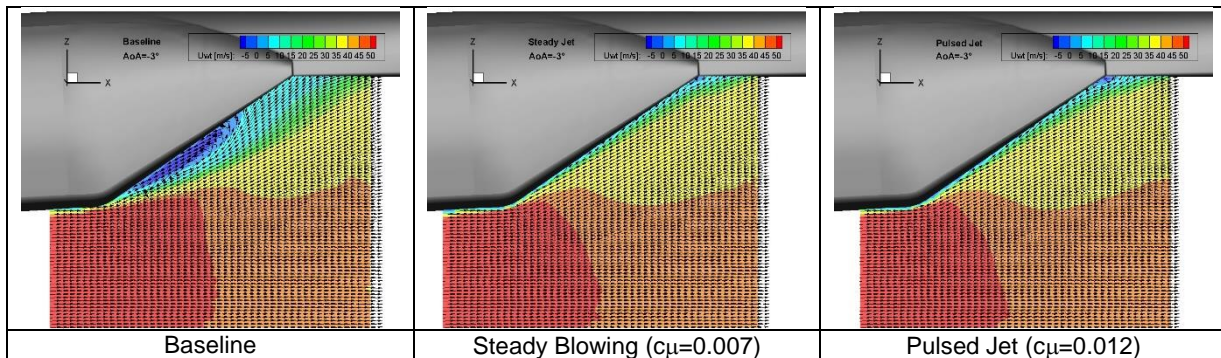Figure 22: Pulsed Jet effect on the sweep yaw angle polar.

| Baseline | Steady Blowing (cμ=0.007) | Pulsed Jet (cμ=0.012) |

Figure 23: Flow velocity contour map comparison: Baseline, steady blowing and pulsed jet at α=-3°.

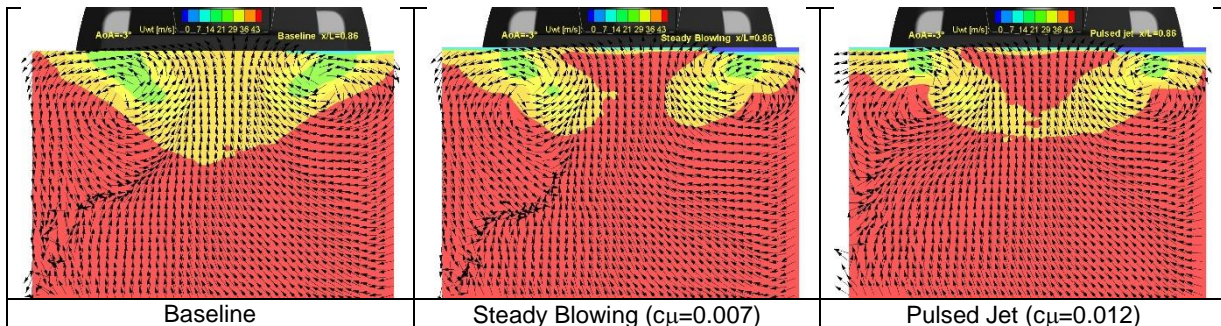| Baseline | Steady Blowing (cμ=0.007) | Pulsed Jet (cμ=0.012) |

Figure 24: Baseline vs AFCs at α=-3°: cross plane velocity components and U components colour map at x/L=0.81:

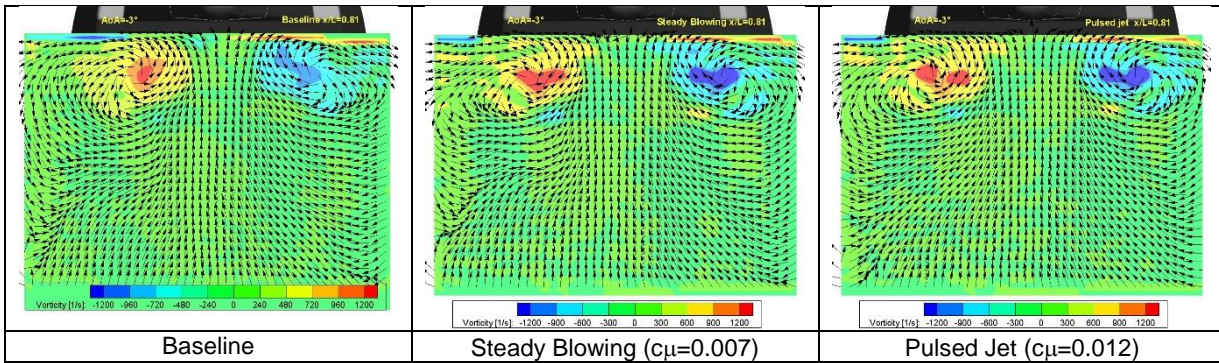| Baseline | Steady Blowing (cμ=0.007) | Pulsed Jet (cμ=0.012) |

Figure 25: Baseline vs AFCs at α=-3°: cross plane velocity vectors and vorticity colour map at x/L=0.81:

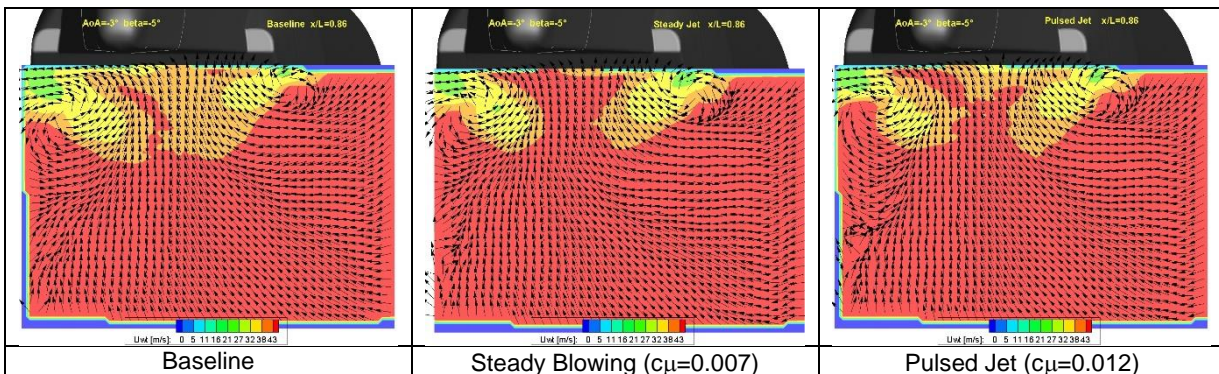| Baseline | Steady Blowing (cμ=0.007) | Pulsed Jet (cμ=0.012) |

Figure 26: Baseline vs AFCs at β=-5°: cross plane velocity vectors and U-component colour map at x/L=0.81:

5.5. AFC2 : Steady Blowing Actuator Results

Few tests were performed on the second configuration and only the steady blowing actuator was investigated. The steady jet blowing from the lateral and the central bottom slots were operated at flow rate of Q=40m^3/h corresponding to a blowing coefficient of cμ=0.002. The continuous jet generates a drag reduction ranging between the 5 to 26 % with respect to the CD0 value. The diagram shows for comparison the AFC1 steady blowing behaviour as well. The second configuration reached analogous drag reduction, if not slightly better, of the AFC1 using the 50% of flow rate. The behaviour of the lift and pitching moments are comparable to the results obtained blowing from the ramp bottom. Although the investigated configuration presented at higher flow rate values a considerable increment of the drag, the use of the lateral slot in order to prevent the formation of the longitudinal vortices and to force a full eddy flow is promising solution for reducing the fuselage download as discussed lately by Schaeffler et al. [23].
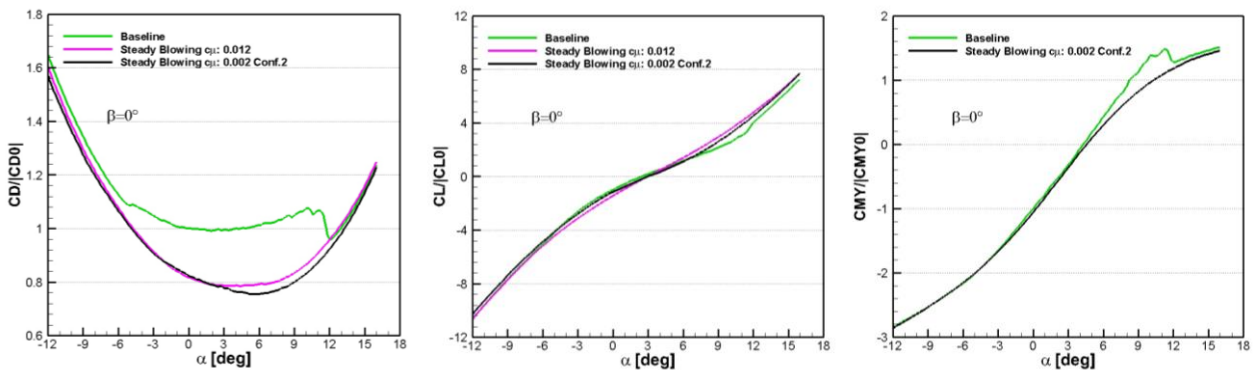

Figure 27: Steady blowing actuator contribution on the normalised aerodynamic coefficients

6. Conclusions

A comprehensive test campaign was successfully performed at the RUAG LWTE wind tunnel aimed to investigate the possibility to reduce the helicopter fuselage passive drag by means of different flow control systems. Two types of AFC systems were designed, manufactured and tested: steady blowing and pulsed jets operating from the bottom of the rear fuselage hatch and from the lateral edges.

The comprehensive test campaign has foreseen the following activities:

• Aerodynamic model force and moments measurements;

• Model surface pressure characterization;

• Flow structures visualization on the rear region of the fuselage by means of mini tuft;

• Wake flow field measurements by 2C and 3C PIV measurements.

Both the investigated flow control systems provided remarkable results in terms of drag reductions without almost any detriments of the other aerodynamic quantities. For some cases an increment of the lift coefficient and of the longitudinal stability was suffered.

The flow control systems were effective for all the incidence and yaw angles investigated.

The active flow control systems were successful for values of the blowing coefficient much smaller respect the values encountered in the literature [14] and [16] and with respect to the values measured during the previous laboratory test [21].

The following main results are reported:

1. The steady blowing actuators, operated from the ramp bottom at different flow volume rate of Q=50, 60 and 80 m^3/h, corresponding to a value of the blowing coefficient of c_μ=0.005, 0.007 and 0.012, induce a model drag reduction with respect to the baseline configuration between the 5 to 23 % for the complete incidence model range (-12° < α < 16°).

2. The steady blowing actuator generates a remarkable benefit in terms of lift download reduction up to 100% for the total angle of attack range except between -5°<α< +2° where the lift download can increases up to a maximum of 50%.

3. Some consideration can be drawn also regarding the effect of the steady jet on the pitching moment behaviour. The steady blowing actuator generates a benefit increasing the stability of the fuselage. Mostly the pitching moment coefficient decreases with respect to the baseline and it presents an advantage in term of longitudinal stability.

4. The steady blowing system presents benefits in terms of aerodynamic coefficients also for the complete beta sweep polar (-15° < β < 15°). In particular the results show a drag reduction with respect to the baseline configuration between 6 to 16 %, benefits and some drawback are encountered for the lift coefficients and reduction of the pitching moment diagram slopes increasing the longitudinal stability.

5. The steady jet actuators, operated form the side ramp (second configuration) at flow volume rate of Q=40 m^3/h corresponding to a value of the blowing coefficient of c_μ=0.002, induce a model drag reduction with respect to the baseline configuration ranging between 5 to 26 %.

6. The pulsed jet actuator, operated form the ramp bottom at flow volume rate of Q=60 m^3/h (corresponding to a total blowing coefficient of c_μ=0.012) and jet frequency of f_j=140 Hz, induces a model drag reduction with respect to the baseline configuration between 4 to 24% for the incidence model range of -12° < α < 12°. For values of α > 12° a small increment of 0.5 drag count is present.

7. The Pulsed Jet actuator induces a remarkable benefit in terms of lift download reduction up to 100% for the total angle of attack range except between -7°<α< +6° where the lift download can increases up to a maximum of 70%. Respect the steady blowing the lift detriment is increased.

8. Analogous, the pulsed jets induce a model drag reduction with respect to the baseline configuration between 8 to 20% also for the complete beta sweep polar (-15° < β < 15°).

9. The pressure measurements clearly indicate a flow separation reduction and an increment of the pressure recovery on the loading ramp due to the flow control systems.

10. The flow field measurements indicate clear wake alleviation in terms of size and momentum loss due to the flow control systems

11. The vortices development for the different model attitudes has been measured and vortex growth and the dissipation phenomena can be investigated.

12. A valuable contribution to the experimental data base has been generated with the flow field measurements for future comparison with the CFD simulations.

Additional data analysis activity is foreseen for the future together experimental/CFD data comparison.

References

[1] Stroub RH and Rabbot JP 1975 Wasted Fuel anaother reason for Drag Reduction, 31 AHS Washington

[2] Gatard J, Costes M, Kroll N, Renzoni P, Kokkalis A, Rocchetto A, Serr C, Larrey E, Filippone A, and Wehr D 1997 High Reynolds Number Helicopter Fuselage Test in the ONERA F1 Pressurized Wind Tunnel in 23rd European Rotorcraft Forum Paper 167 September 16-18, Dresden, Germany

[3] Renaud T, Le Pape A and Pèron S, 2012 Numerical Analysis of Hub and Fuselage Drag Breakdown of a Helicopter Configuration in 38th European Rotorcraft Forum, September 4-7 Amsterdam, The Netherlands

[4] Grawunder M, Reß R, Breitsamter C and Adams N A 2012 Flow Characteristics of a Helicopter Fuselage Configuration Including a Rotating Rotor Head, in 28th int. congress of the aeronautical sciences, September 23-28, Brisbane, Australia

[5] Ahmed S R 1983 Influence of base slant on the wake structure and drag of road vehicles. J. Fluids Eng. 105, 429–434

[6] Seddon J 1990 Basic helicopter aerodynamics BSP Professional books ISBN 0-632-02032-6.

[7] Batrakov A S, Kusyumov A N, Mikhailov S A, Pakhov V V, Sungatullin A R, Zherekhov V V and Barakos G N 2013 A Study in Helicopter Fuselage Drag in 39th European Rotorcraft Forum, September 3-6 Moskow, Russia

[8] Reß R, Grawunder M, Breitsamter C 2014 Parasite Drag Reduction od a Twin Engine Lightweight Helicopter Configuration, In: DGLRK2014–0046, German Aerospace Congress, Augsburg, 16.-18. Sept. 2014, pp. 1-9

[9] Breitsameter C, Grawunder M and Reß R Aerodynamic dsign optimization for a helicopter configuration including a rotating head in 29th int. congress of the aeronautical sciences, September 7-12, San Petersburg, Russia ICAS 2014_0686_paper

[10] Gad-el-Hak M 1996 Modern Developments in Flow Control. in Applied Mechanics Reviews, vol. 49, pp. 365–379

[11] Joslin R D and Miller D N 2009 Fundamentals and Applications of Modern Flow Control American Institute of Aeronautics & Astronautics Vol. 231 of Progress in astronautics and aeronautics Ed.

[12] Martin PB, Tung C, Hassan AA, Cerchie D, Roth J, Active Flow control Measurements and CFD on a transport Helicopter fuselage, proc. of American Helicopter Society 61st Annual Forum, Paper 61, Grapevine, TX, 2005

[13] Eli Ben-Hamou, Eran Arad & Avi Seifert, Generic Transport Aft-body Drag Reduction using Active Flow Control, Flow Turbulence Combust (2007) 78:365–382, DOI 10.1007/s10494-007-9070-x.

[14] Schaeffler N W, Allan B G, Lienard C and Le Pape A 2010 Progress Towards Fuselage Drag Reduction via Active Flow Control: A Combined CFD and Experimental Effort, presented at 36th European Rotorcraft Forum, September 7-9 Paris

[15] Allan B G and Schaeffler N W 2011 Numerical Investigation of Rotorcraft Fuselage Drag Reduction using Active Flow Control presented at the American Helicopter Society 67th Annual Forum, Paper 111, Virginia Beach, VA, 2011 NTRS

Document ID: 20110011552.

[16] Le Pape A, Lienard C, Verbeke C, Pruvost M and De Coninck J L 2013 Helicopter Fuselage Drag Reduction Using Active Flow Control: a Comprehensive Experimental investigation. Journal of the American Helicopter Society, Vol. 60, 2015, pp. 032003:1–032003:12, doi:10.4050/JAHS.60.032003.

[17] Crittenden T, Glezer A, Funk R, Parekh D (2001) Combustion-Driven Jet Actuators for Flow Control. AIAA Paper 2001-2768

[18] George T. K. Woo, Ari Glezer, Jeremy Bain, and Lakshmi Sankar, Rotorcraft Fuselage Drag Reduction Using Combustion Powered Actuators, 49th AIAA Aerospace Sciences Meeting including the New Horizons Forum and Aerospace Exposition, Orlando, Florida, 4-7 January 2011.

[19] Woo GTK, Glezer A, Crittenden TM, Transitory Separation Control on a ROBIN Fuselage using Pulsed Actuation, in 37th ERF conference, Gallarate, Italy, 13-15 September, 2011.

[20] Martin PB, Overmeyer AD, Tanner PE, Wilson JS and Jenkins LN, Helicopter Fuselage Active Flow Control in the Presence of a Rotor, in proceedings of American Helicopter Society 70th Annual Forum, Paper 335, Montreal, Quebec, Canada, 2014.

[21] De Gregorio F. and Vitagliano P.L. Experimental And Numerical Investigation of Helicopter Fuselage Model With Active Flow Control in proc. 40th European Rotorcraft Forum, Paper 23-ASeptember 2-5, 2014, Southampton, UK

[22] Barlow J W Rae WH and Pope A 1999 Wind Tunnel Testing 3rd edition, John Wiley & Sons, Inc.

[23] Schaeffler N W, Allan B G, Jenkins L N, Yao C S, Bartram S M, Mace W D, Wong O D, Tanner P E, Mechanism of Active Aerodynamic Load Reduction on a Rotorcraft fuselage with Rotor Effects Presented at the American Helicopter Society Technical Meeting on Aeromechanics Design for Vertical Lift, San Francisco, CA, January 20-22, 2016